Int. J. Heat Mass Transfer. Vol. 11, pp. 1513–1534. Pergamon Press 1968. Printed in Great Britain

THEORETICAL RESULTS FOR VARIABLE PROPERTY, LAMINAR BOUNDARY LAYERS IN WATER WITH ADVERSE PRESSURE GRADIENTS

G. POOTS and G. F. RAGGETT
Department of Applied Mathematics, The University of Hull, England

(*Received* 27 *November* 1967 *and in revised form* 18 *March* 1968)

Abstract—Numerical solutions of the two-dimensional laminar boundary-layer equations for flows with heat transfer and adverse pressure gradient are presented for water. Experimental values (in the range 0–100°C) for the viscosity, conductivity, specific heat and density are used. On introducing the Howarth–Dorodnitsyn and Görtler transformations the boundary-layer equations are put in a form suitable for numerical work. The resulting pair of coupled partial differential equations are solved, using the implicit method of Hartree and Womersley, first for the flow past a flat plate with main stream velocity $u_m = u_0 (1 - x/8c)$ and secondly for the potential flow past a circular cylinder with main stream velocity $u_m = u_0 \sin(x/c)$. Boundary-layer characteristics such as displacement and momentum thicknesses, skin friction and heat-transfer coefficients are evaluated up to the point of separation. The effect of variable fluid properties is to move the position of separation either upstream or downstream of the known incompressible isothermal flow location depending on whether the wall is cooled or heated. For example, with main stream velocity $u_m = u_0 (1 - x/8c)$ the numerical evidence obtained indicates that separation is likely to occur at approximately $x_s/c = 0{\cdot}959\,(Pr_m/Pr_w)^{\frac{1}{4}}$. In the case $u_m = u_0 \sin(x/c)$ the approximate location is given by $x_s/c = \pi/2 + 0{\cdot}25\,(Pr_m/Pr_w)^{\frac{1}{4}}$. Here Pr_w and Pr_m are, respectively, the wall and main stream Prandtl numbers.

NOMENCLATURE

c, representative length [cm];
c_p, specific heat at constant pressure [cal/g dec C];
C_f, dimensionless skin friction coefficients;
f, dimensionless velocity function at $x/c = 0$;
F, dimensionless velocity function;
h, mesh length in the η-direction;
k, thermal conductivity [cal/cm/s deg C];
Nu_x, local Nusselt number;
p, pressure;
Pr, $= \mu c_p/k$, Prandtl number;
Re_{m_x}, $= \rho u_m\, x/\mu$, Reynolds number;
T, temperature [°C];
u, v, velocity components [cm/s];
x, y, coordinates along and perpendicular to the wall [cm];
X, Y, Howarth–Dorodnitsyn variables, see equation (7).

Greek symbols

δ_1, δ_2, boundary-layer thicknesses [cm];
μ, viscosity [g/cm s];
τ, shear stress;
θ, dimensionless temperature function at $x/c = 0$;
Θ, dimensionless temperature function;
λ, $= (\xi_{i+1} + \xi_i)/(\xi_{i+1} - \xi_i)$;
ρ, density [g/cm^3];
ξ, η, Görtler variables [see equation (8)];
ψ, stream function.

Subscripts

i, j, finite difference mesh point;
m, main stream condition;
M, number of iterations;

N, number of mesh points in the η-direction;
s, separation point condition;
w, wall condition.

1. INTRODUCTION

SEVERAL theoretical investigations have been made on the effect of variable fluid properties on flow and heat transfer in a laminar boundary layer in liquids. On assuming that the viscosity of the liquid varies with the temperature and all other properties are independent of the temperature Schuh [1] has considered the flow past a semi-infinite flat plate with zero pressure gradient. The plate was maintained at a temperature different from that of the mainstream and the viscosity temperature dependence was chosen as

$$\mu/\mu_w = \left(\frac{T_w + T_c}{T + T_c}\right)^b,$$

where b and T_c are constants. Schuh solved the relevant similarity equations by employing an iterative technique. Later Seban [2] showed how this boundary value problem could be converted to an initial value problem by means of a well known transformation due to Töpfer (see Curle [3]). Seban extended the numerical work of Schuh and gave information for a wide range of values of the parameter μ_w/μ_m, the ratio of wall to mainstream viscosity, and for various values of the wall Prandtl number. The model liquid mainly considered was one with exponent $b = 3$. In particular when $Pr_w = 10$ and $0{\cdot}2 \leqslant \mu_w/\mu_m \leqslant 4{\cdot}4$ Seban's results indicated that heat-transfer coefficients varied by at most $+14$ per cent from those determined employing a constant fluid property model based on the wall temperature as the reference temperature; skin friction coefficients varied from -14 to 19 per cent from constant fluid property values based on the mainstream temperature as the reference temperature. It was further established that gross effects of the variable viscosity was controlled by the mainstream Prandtl number since this gave the degree of penetration of the thermal boundary layer into the liquid.

From the results of Seban quantitative information could be obtained for a particular liquid and specific wall and mainstream temperatures deduced by means of a suitable interpolation procedure. However, from a computational viewpoint, it is probably more economical to solve the generalized Blasius equations directly by an iterative procedure, say, employing the Runge–Kutta method. Such calculations have been performed by Poots and Raggett [4] for the laminar boundary layer on a flat plate in water. Experimental values (in the range 0–100°C) for the viscosity, conductivity, specific heat and density were employed. These results indicated that in the case of a heated wall with $T_m = 0$°C and T_w varying from 0 to 100°C the dimensionless Nusselt number $Nu/Re_m^{\frac{1}{2}}$ can increase by as much as 31 per cent, whilst the dimensionless skin friction coefficient $C_f Re_m^{\frac{1}{2}}$ can decrease by at most 33 per cent. For a cooled wall with $T_m = 100$°C and T_w varying from 100°C to °C there is a possible reduction of 12 per cent in $Nu/Re_m^{\frac{1}{2}}$ and an increase of 20 per cent in $C_f Re_m^{\frac{1}{2}}$. These trends are in agreement with the work of Schuh and Seban and further demonstrate that maximum deviations from the constant fluid property model occur when the wall is heated. In [4] the effect of variable fluid properties on the steady rotationally symmetric flow in the presence of an infinite rotating disk in quiescent fluid was also examined. Here again maximum deviations of the heat transfer and moment coefficients from the corresponding constant fluid property values occur when the disk is heated.

It would be desirable to have theoretical information on the effect of variable physical properties on flows with adverse pressure gradient. For compressible flow with heat transfer and adverse pressure gradient of a model gas, with Prandtl number unity and viscosity increasing linearly with increasing temperature, it is known (see Stewartson [5]) that heating the wall produces an earlier separation of the boundary layer. In the boundary-layer flow with adverse pressure gradient in water, where

the viscosity decreases with increasing temperature, it is to be anticipated that heating the wall will delay separation.

The object of this paper is to report on theoretical results obtained on the numerical integration of the two-dimensional boundary-layer equations with adverse pressure gradient and heat transfer in water. Two flow regimes are considered for various wall and main stream temperature differences. Following previous investigations the first example to be examined is the flow past a semi-infinite flat plate placed edgewise to a stream with velocity $u_m = u_0(1 - x/8c)$, where c is a representative length and x is measured from the leading edge. The corresponding numerical solution for the isothermal boundary layer in incompressible flow has been considered by Howarth [6], Hartree [7] and Leigh [8]; asymptotic solutions in the upstream neighbourhood of the point of separation have been investigated by Goldstein [9], Jones [10], Terrill [11] and Stewartson [12]. Related compressible flows of a model gas (with $Pr = 1$, $\mu \propto T$) hâve been considered numerically by Curle [13] and Poots [14]; the analytic behaviour of these solutions in the vicinity of a point of vanishing wall shear stress has been considered by Stewartson [15]. The second example considered is for the flow with mainstream velocity $u_m = u_0 \sin(x/c)$ corresponding to the incompressible potential flow past a circular cylinder of radius c; x being measured from the forward stagnation point. Information on the incompressible isothermal boundary layer is available from the work of Terrill [11].

In this investigation the two-dimensional boundary-layer equations are put in a form more amenable to numerical analysis on introducing the Howarth–Dorodnitsyn and Görtler transformations. The implicit procedure of Hartree and Womersley (see Hartree [7]) is employed in the numerical integration of the resulting pair of coupled parabolic partial differential equations, the details of which are given in the Appendix.

It must be emphasized that from these numerical solutions it is not possible to give a precise location of the point of separation, where $(\partial u/\partial y)_w = 0$. Indeed, as in the numerical integrations for the constant fluid property model discussed in [6–9], there is a breakdown in the numerical process in the neighbourhood of vanishingly small skin friction. However, in this case it has been established [9–12], that the breakdown was due to an algebraic singularity of the form $(\partial u/\partial y)_w \sim (x - x_s)^{\frac{1}{2}}$ where $x = x_s$ is the point of separation. No such theory can be envisaged for the type of variable fluid property model proposed in the present paper. Thus there would appear to be some justification for examining the analytic behaviour of the flow at a point of zero skin friction with heat transfer using a simplified variable fluid property model applicable to liquids of the form:

$$\left.\begin{aligned} &\rho = \rho_m, \qquad c_p = c_{p_m}, \\ &\frac{1}{\mu} = \frac{1}{\mu_w} + \left(\frac{T - T_w}{T_m - T_w}\right)\left(\frac{1}{\mu_m} - \frac{1}{\mu_w}\right), \\ &k = k_w + \left(\frac{T - T_w}{T_m - T_w}\right)(k_m - k_w). \end{aligned}\right\} \quad (1)$$

This investigation would perhaps follow closely that of Stewartson [15] for the compressible boundary layer with adverse pressure gradient. In the case of a model gas with $\mu \propto T$ and $Pr = 1$ Stewartson has shown that the boundary layer can only develop a singularity at a point of zero skin friction if the heat transfer at this point is zero. Stewartson also shows that this conclusion is true for a real gas. In the absence of information of this type for a variable fluid property model given by expressions (1) it is impossible to fully appreciate the behaviour of liquid flows from the numerical solutions alone, especially when these cannot be extended beyond an estimated value of x_s at which breakdown in the numerical process occurs. In general at this value of x_s the wall gradient $(\partial u/\partial y)_w$ is small and it is assumed that at $x = x_s$ boundary-layer separation occurs. Thus results are presented on the effect of heating or cooling the wall on flow and heat-transfer characteristics from the

point of attachment at $x = 0$ up to the approximate location of the point of separation at $x = x_s$. In particular information is obtained on the effect of variable fluid properties on the location of x_s.

2. THE TWO-DIMENSIONAL LAMINAR BOUNDARY-LAYER EQUATIONS

The governing equations of conservation of mass, momentum and thermal energy in a two-dimensional steady laminar boundary layer are, respectively,

$$\frac{\partial}{\partial x}(\rho u) + \frac{\partial}{\partial y}(\rho v) = 0, \tag{2}$$

$$\rho\left(u\frac{\partial u}{\partial x} + v\frac{\partial u}{\partial y}\right) = \rho_m u_m \frac{\mathrm{d}u_m}{\mathrm{d}x} + \frac{\partial}{\partial y}\left(\mu\frac{\partial u}{\partial y}\right), \tag{3}$$

and

$$\rho c_p\left(u\frac{\partial T}{\partial x} + v\frac{\partial T}{\partial y}\right) = \frac{\partial}{\partial y}\left(k\frac{\partial T}{\partial y}\right). \tag{4}$$

Here u and v denote the velocity components in the x and y directions, x being measured along the surface and y along a normal; T is the local temperature and $u_m(x)$ is the mainstream velocity. In these equations the gravitational body force, viscous dissipation and work done against compression have been neglected (see, for example, [4]).

The boundary conditions are:

$$\left.\begin{aligned} &u = v = 0, \quad T = T_w \quad \text{at } y = 0, \quad x \geqslant 0, \\ &u \to u_m(x), \quad T \to T_m \quad \text{as } y \to \infty, \quad x \geqslant 0. \end{aligned}\right\} \tag{5}$$

At present the remaining conditions at $x = 0$, $0 \leqslant y \leqslant \infty$ are not specified as they depend on the geometrical shape of the surface and its orientation to the free stream direction. To complete the above set of equations (2–5) it is assumed that the variation of the liquid properties with temperature is known from experiment.

Introducing the stream function ψ defined by

$$\rho u = \rho_m \partial\psi/\partial y, \qquad \rho v = -\rho_m \partial\psi/\partial x, \tag{6}$$

the Howarth–Dorodnitsyn variables:

$$X = x, \qquad Y = \int_0^y \frac{\rho}{\rho_m}\,\mathrm{d}y, \tag{7}$$

the Görtler transformation (see Curle [3]):

$$\left.\begin{aligned} \xi &= \frac{\rho_m}{\mu_m}\int_0^X u_m(X)\,\mathrm{d}X, \\ \eta &= Y u_m(X)\Big/\left\{2\frac{\mu_m}{\rho_m}\int_0^X u_m(X)\,\mathrm{d}X\right\}^{\frac{1}{2}}, \end{aligned}\right\} \tag{8}$$

and the new dimensionless variables F and Θ, such that

$$\left.\begin{aligned} \psi &= \frac{\mu_m}{\rho_m}(2\xi)^{\frac{1}{2}} F(\xi, \eta), \\ T &= T_w + (T_m - T_w)\,\Theta(\xi, \eta), \end{aligned}\right\} \tag{9}$$

the boundary-layer equations (2–4) now reduce to

$$\frac{\partial}{\partial\eta}\left(\frac{\rho\mu}{\rho_m\mu_m}\frac{\partial^2 F}{\partial\eta^2}\right) + F\frac{\partial^2 F}{\partial\eta^2} + \beta(\xi)\left\{\frac{\rho_m}{\rho} - \left(\frac{\partial F}{\partial\eta}\right)^2\right\} = 2\xi\left\{\frac{\partial F}{\partial\eta}\frac{\partial^2 F}{\partial\xi\partial\eta} - \frac{\partial F}{\partial\xi}\frac{\partial^2 F}{\partial\eta^2}\right\}, \tag{10}$$

and

$$\frac{\partial}{\partial\eta}\left(\frac{\rho k}{\rho_m k_m}\frac{\partial\Theta}{\partial\eta}\right) + Pr_m\frac{c_p}{c_{p_m}}F\frac{\partial\Theta}{\partial\eta} = 2\xi\, Pr_m\frac{c_p}{c_{p_m}}\left\{\frac{\partial F}{\partial\eta}\frac{\partial\Theta}{\partial\xi} - \frac{\partial F}{\partial\xi}\frac{\partial\Theta}{\partial\eta}\right\}, \tag{11}$$

where

$$\beta(\xi) = 2\xi\xi''/(\xi')^2, \tag{12}$$

the dash denoting differentiation with respect to X. The velocity field is related to F by

$$u = u_m\,\partial F/\partial\eta,$$

$$v = -\frac{\rho_m}{\rho}\left\{(2\xi)^{\frac{1}{2}}\xi\frac{\mu_m}{\rho_m}\left(\frac{F}{2\xi}+\frac{\partial F}{\partial \xi}\right.\right.$$
$$\left.\left.+(\beta-1)\frac{\eta}{2\xi}\frac{\partial F}{\partial \eta}\right)+u\left(\frac{\partial Y}{\partial x}\right)_y\right\}. \quad (13)$$

The boundary conditions (5) transform to

$$F = \partial F/\partial\eta = 0, \quad \Theta = 0, \quad \text{at} \quad \eta = 0, \quad \xi \geqslant 0$$
$$\partial F/\partial\eta \to 1, \quad \Theta \to 1 \quad \text{as} \quad \eta \to \infty, \quad \xi \geqslant 0. \quad (14)$$

Note that the main advantages, from the viewpoint of numerical computation, of introducing the transformations (7) and (8) can best be seen on considering the final form of the transformed boundary-layer equations (10) and (11) subject to the boundary conditions (14). The Howarth–Dorodnitsyn transformation enables the stream function ψ to be introduced in a concise manner and so avoiding, in particular, the occurrence of partial derivatives of ρ with respect to x and y. When the Görtler transformation is employed the mainstream velocity only enters the equations explicitly in the form of $\beta(\xi)$ and, moreover, the boundary conditions on F are standardized. The latter, as will be seen in the Appendix, produces some simplification in the formal development of an iterative matrix scheme to be employed in the solution of (10) and (11).

It remains to specify the two different flow configurations to be considered.

Flow past a flat plate

Consider the flow past a flat plate placed edgewise to an incident stream when an adverse pressure gradient is superimposed. The plate is defined by $y = 0$, $x \geqslant 0$ and the main stream velocity distribution is chosen as

$$u_m = u_0(1 - x/8c); \quad (15)$$

the plate is maintained at temperature T_w and the main stream temperature is denoted by T_m. Thus the boundary conditions at the leading edge are:

$$u = u_0, \quad T = T_m \quad \text{at} \quad x = 0, \quad y > 0. \quad (16)$$

In terms of the F and Θ variables these yield, since $\beta(\xi) \to 0$ as $\xi \to 0$, the conditions:

$$F(0,\eta) = f(\eta), \quad \Theta(0,\eta) = \theta(\eta), \quad (17)$$

where $f(\eta)$ and $\theta(\eta)$ satisfy the differential equations:

$$\frac{d}{d\eta}\left(\frac{\rho\mu}{\rho_m\mu_m}\frac{d^2f}{d\eta^2}\right)+f\frac{d^2f}{d\eta^2}=0, \quad (18)$$

$$\frac{d}{d\eta}\left(\frac{\rho k}{\rho_m k_m}\frac{d\theta}{d\eta}\right)+Pr_m\frac{c_p}{c_{p_m}}f\frac{d\theta}{d\eta}=0. \quad (19)$$

The appropriate boundary conditions are:

$$\left.\begin{aligned} f = \frac{df}{d\eta} = \theta = 0 \quad &\text{at} \quad \eta = 0, \\ \frac{df}{d\eta} \to 1, \quad \theta \to 1 \quad &\text{as} \quad \eta \to \infty. \end{aligned}\right\} \quad (20)$$

The above equations (18–20) determine the variable fluid property generalization of the classic Blasius–Pohlhausen flow past a flat plate with heat transfer and zero pressure gradient. In [4] numerical results of these similarity solutions for various combinations of wall and main stream temperatures, are given for water.

The transformed boundary-layer equations (10) and (11) must now be solved subject to the conditions (14) and (17); $\beta(\xi)$ as defined in (12) is determined using expression (15). For an isothermal flow (when $T_w = T_m$) equation (10) reduces to that for the constant fluid property model which has been considered in detail by Howarth [6], Hartree [7] and Leigh [8]. In this case the boundary layer separates at $x_s/c = 0{\cdot}95854$ and in the upstream neighbourhood of the separation point $(\partial u/\partial y)_w \sim (x - x_s)^{\frac{1}{2}}$ (see the work of Goldstein [9], Jones [10], Terrill [11] and Stewartson [12] for details).

Potential flow past a circular cylinder

A circular cylinder is maintained at constant temperature T_w. The incident free stream at

temperature T_m flows in a direction perpendicular to the axis of the cylinder. The main stream potential flow is given by

$$u_m = u_0 \sin(x/c), \tag{21}$$

where $u_0 = 2u_\infty$, u_∞ being the undisturbed free stream velocity at large distances from the cylinder. Here x is measured round the cylinder from the forward stagnation point and c is the radius of the cylinder. As $x \to 0$, $\beta(\xi) \to 1$ and so

$$F(0, \eta) = f(\eta), \qquad \Theta(0, \eta) = \theta(\eta), \tag{22}$$

where f and θ satisfy the differential equations:

$$\frac{\mathrm{d}}{\mathrm{d}\eta}\left(\frac{\rho\mu}{\rho_m\mu_m}\frac{\mathrm{d}^2 f}{\mathrm{d}\eta^2}\right) + f\frac{\mathrm{d}^2 f}{\mathrm{d}\eta^2} + \left(\frac{\rho_m}{\rho} - \left(\frac{\mathrm{d}f}{\mathrm{d}\eta}\right)^2\right) = 0, \tag{23}$$

and

$$\frac{\mathrm{d}}{\mathrm{d}\eta}\left(\frac{\rho k}{\rho_m k_m}\frac{\mathrm{d}\theta}{\mathrm{d}\eta}\right) + Pr_m \frac{c_p}{c_{p_m}} f\frac{\mathrm{d}\theta}{\mathrm{d}\eta} = 0, \tag{24}$$

subject to the boundary conditions given in (19).

The similarity solution for the two-dimensional stagnation point has been investigated in detail for the constant fluid property model, $T_w \to T_m$; flow and heat-transfer characteristics are known for a wide range of Prandtl numbers (see Curle [3]). To date the results on the similarity solutions for water with variable fluid properties are not available in the literature. However, some representative numerical solutions have been obtained, using an iterative matrix scheme given in the Appendix, and these will be discussed later.

For the potential flow past a circular cylinder the transformed boundary-layer equations (10) and (11) are now solved subject to the boundary conditions (14) and (22); $\beta(\xi)$ as defined in (12) is determined using expression (21). The constant fluid property model equation obtained on letting $T_w \to T_m$ in (10) has already been considered by Terrill [11]. Terrill gives numerical results on velocity profiles, displacement and momentum thicknesses, and wall skin friction as a function of the distance from the forward stagnation point; the point of separation was located by Terrill at $x_s/c = 1{\cdot}822983$ rad. Terrill also investigates the analytical properties of this solution upstream of the separation point.

3. FLOW AND HEAT-TRANSFER CHARACTERISTICS

Before presenting a discussion of the numerical results it is convenient at this stage to collect definitions of certain flow and heat-transfer characteristics. In terms of the Howarth–Dorodnitsyn and Görtler variables the wall shear stress is

$$\tau_w = \mu_w\left(\frac{\partial u}{\partial y}\right)_{y=0} = \mu_w \frac{\rho_w}{\rho_m^2} \times \mu_m \frac{\xi'^2}{(2\xi)^{\frac{1}{2}}}(\partial^2 F/\partial\eta^2)_0; \tag{25}$$

the related dimensionless skin friction coefficient C_{f_x} is

$$C_{f_x} = \tau_w/\tfrac{1}{2}\rho_m u_m^2(x). \tag{26}$$

The local wall Nusselt number is given by

$$Nu_x = x(\partial T/\partial y)_0/(T_m - T_w) = x\frac{\xi'}{(2\xi)^{\frac{1}{2}}}\frac{\rho_w}{\rho_m}\left(\frac{\partial\Theta}{\partial\eta}\right)_0, \tag{27}$$

and the local Reynolds number, based on main stream properties, is defined as

$$Re_{m_x} = \rho_m u_m(x)\, x/\mu_m. \tag{28}$$

It is useful to evaluate some overall measures of the fluid boundary-layer thickness. These are the displacement thickness

$$\delta_{1_x} = \int_0^\infty \left(1 - \frac{\rho u}{\rho_m u_m}\right)\mathrm{d}y = \frac{(2\xi)^{\frac{1}{2}}}{\xi'}\int_0^\infty \frac{\rho_m}{\rho}\left(1 - \frac{\rho}{\rho_m}\frac{\partial F}{\partial\eta}\right)\mathrm{d}\eta, \tag{29}$$

and the momentum thickness

$$\delta_{2_x} = \int_0^\infty \frac{\rho u}{\rho_m u_m}\left(1 - \frac{u}{u_m}\right) dy = \frac{(2\xi)^{\frac{1}{2}}}{\xi'} \int_0^\infty \frac{\partial F}{\partial \eta}\left(1 - \frac{\partial F}{\partial \eta}\right) d\eta. \quad (30)$$

In non-dimensional form the above relations become:

$$C_{f_x} Re_{m_x}^{\frac{1}{2}} = \alpha_1 \left(\frac{x}{c}\right) s\left(\frac{x}{c}\right), \quad (31)$$

$$Nu_x/Re_{m_x}^{\frac{1}{2}} = \alpha_2 \left(\frac{x}{c}\right) s\left(\frac{x}{c}\right), \quad (32)$$

$$\delta_{1_x} Re_{m_x}^{\frac{1}{2}}/x = \alpha_3 \left(\frac{x}{c}\right) \Big/ s\left(\frac{x}{c}\right), \quad (33)$$

and

$$\delta_{2_x} Re_{m_x}^{\frac{1}{2}}/x = \alpha_4 \left(\frac{x}{c}\right) \Big/ s\left(\frac{x}{c}\right). \quad (34)$$

In expressions (31) to (34)

$$\alpha_1 = \sqrt{2}\frac{(\rho\mu)_w}{(\rho\mu)_m}(\partial^2 F/\partial\eta^2)_0, \quad (35)$$

$$\alpha_2 = \frac{1}{\sqrt{2}}\frac{\rho_w}{\rho_m}(\partial\Theta/\partial\eta)_0, \quad (36)$$

$$\alpha_3 = \sqrt{2}\int_0^\infty \frac{\rho_m}{\rho}\left(1 - \frac{\rho}{\rho_m}\frac{\partial F}{\partial \eta}\right) d\eta \quad (37)$$

and

$$\alpha_4 = \sqrt{2}\int_0^\infty \frac{\partial F}{\partial \eta}\left(1 - \frac{\partial F}{\partial \eta}\right) d\eta. \quad (38)$$

The function $s(x/c)$ is determined by the shape of the immersed body and the free stream conditions. For the flat plate with retarded main stream velocity $u_m = u_0(1 - x/8c)$:

$$s\left(\frac{x}{c}\right) = \sqrt{[(1 - x/8c)/(1 - x/16c)]}; \quad (39)$$

for the potential flow past a circular cylinder with $u_m = u_0 \sin(x/c)$:

$$s\left(\frac{x}{c}\right) = \sqrt{\left[\frac{x}{c}\cot\left(\frac{x}{2c}\right)\right]}. \quad (40)$$

4. NUMERICAL SOLUTIONS FOR WATER

Property values. The physical properties are taken to be those for saturated water at the appropriate temperatures. The data for water are taken from tables compiled by Mayhew and Rogers [16]. In cgs units these experimental values are adequately represented, as discussed in [17], by algebraic expressions in T; for example:

$$\mu = \exp \sum_{i=0}^{10} C_i\{[T_w + (T_m - T_w)\Theta(\xi, \eta) - 50°C]/50°C\}^i.$$

Solutions. Numerical solutions of the boundary-layer equations are obtained for the flat plate with retarded main stream velocity $u_m = u_0(1 - x/8c)$ for the following wall and main stream temperatures $(T_w, T_m) = (0, 100)$, $(40, 100)$, $(100, 100)$, $(0, 0)$, $(40, 0)$ and $(100, 0)$. For the potential flow past a circular cylinder with $u_m = u_0 \sin(x/c)$ solutions for $(T_w, T_m) = (0, 100)$, $(100, 100)$, $(0, 0)$ and $(100, 0)$ have been obtained. The integration procedure is given in the Appendix. The flow and heat-transfer characteristics $(\partial^2 F/\partial\eta^2)_0$, $(\partial\Theta/\partial\eta)_0$, $\delta_{1_x} Re_{m_x}^{\frac{1}{2}}/x$, $\delta_{2_x} Re_{m_x}^{\frac{1}{2}}/x$, $\delta_{2_x} Re_{m_x}^{\frac{1}{2}}/x$, $C_{f_x} Re_{m_x}^{\frac{1}{2}}/x$ and $Nu_x/Re_{m_x}^{\frac{1}{2}}$ as functions of x/c are given in Tables 1 and 2 for the flat plate and in Tables 3 and 4 for the circular cylinder. These tables have been rounded off to three decimals. Note that in each case the terminal value of x/c is an estimate, to within an error of 0·1 per cent, of the position of breakdown of the numerical integration procedure. In the neighbourhood of this value of x/c the gradient $(\partial u/\partial y)_w$ is small; as previously discussed, it is assumed that boundary-layer separation occurs at this location.

5. RESULTS AND DISCUSSION

The effects of heating or cooling the wall on the flow and heat transfer for the flat plate and circular cylinder will be discussed separately. In the case of the flat plate the variable fluid

Table 1. Flat plate, $u_m = u_0 (1 - x/8c)$

x/c	$\left(\frac{\partial^2 F}{\partial \eta^2}\right)_0$	$\left(\frac{\partial \Theta}{\partial \eta}\right)_0$	$\delta_1 Re_x^{\frac{1}{2}}/x$	$\delta_2 Re_x^{\frac{1}{2}}/x$	$C_{f_x} Re_x^{\frac{1}{2}}$	$Nu_x/Re_x^{\frac{1}{2}}$
			$T_w = 0, T_m = 100$			
0·0	0·0850	0·480	2·780	0·795	0·795	0·354
0·2	0·0696	0·453	2·975	0·817	0·647	0·333
0·3	0·0607	0·438	3·099	0·828	0·562	0·320
0·4	0·0507	0·418	3·254	0·841	0·468	0·304
0·5	0·0390	0·391	3·456	0·854	0·359	0·284
0·6	0·0243	0·351	3·761	0·868	0·223	0·254
0·677	0·006	0·277	4·281	0·879	0·054	0·200
			$T_w = 40, T_m = 100$			
0·0	$0{\cdot}221_5$	0·505	2·239	0·753	0·753	0·370
0·2	0·189	$0{\cdot}482_5$	2·384	0·774	0·639	0·351
0·4	0·150	0·453	2·577	0·798	0·505	0·327
0·6	0·101	0·407	2·869	0·826	0·337	0·292
0·7	0·068	0·370	3·104	0·841	0·226	0·265
0·8	0·011	0·270	3·665	0·857	0·036	0·192
0·803	0·007	0·259	3·708	0·858	0·024	0·185
			$T_w = 100, T_m = 100$			
0·0	0·470	0·569	1·720	0·664	0·664	0·402
0·2	0·414	0·550	1·821	0·684	0·582	0·386
0·4	0·350	0·525	1·947	0·707	0·488	0·366
0·6	0·272	0·491	2·118	0·732	0·377	0·340
0·8	0·170	0·437	2·383	0·762	0·233	0·300
0·9	0·096	0·386	2·616	0·779	0·131	0·265
0·958	0·005	0·283	2·991	0·789	0·007	0·194

Table 2. Flat plate, $u_m = u_0 (1 - x/8c)$

x/c	$\left(\frac{\partial^2 F}{\partial \eta^2}\right)_0$	$\left(\frac{\partial \Theta}{\partial \eta}\right)_0$	$\delta_1 Re_{m_x}^{\frac{1}{2}}/x$	$\delta_2 Re_{m_x}^{\frac{1}{2}}/x$	$C_{f_x} Re_{m_x}^{\frac{1}{2}}$	$Nu_x/Re_{m_x}^{\frac{1}{2}}$
			$T_w = 0, T_m = 0$			
0·0	0·470	1·141	1·720	0·664	0·664	0·801
0·2	0·414	1·093	1·821	0·684	0·582	0·768
0·4	0·350	1·032	1·947	0·707	0·488	0·720
0·6	0·272	0·947	2·118	0·732	0·377	0·657
0·8	0·170	0·812	2·383	0·762	0·233	0·559
0·9	0·096	0·686	2·616	0·779	0·131	0·470
0·958	0·005	0·427	2·991	0·789	0·007	0·292
			$T_w = 40, T_m = 0$			
0·0	1·117	1·315	1·221	0·573	0·575	0·923
0·2	1·022	1·277	1·284	0·592	0·522	0·890
0·4	0·914	1·231	1·359	0·613	0·464	0·853
0·6	0·789	1·174	1·450	0·637	0·398	0·807
0·8	0·641	1·098	1·567	0·663	0·321	0·750
1·0	0·454	0·987	1·731	0·693	0·225	0·669
1·1	0·334	0·903	1·848	0·710	0·165	0·610
1·2	0·170	0·760	2·026	0·728	0·084	0·511
1·246	0·016	0·531	2·221	0·737	0·008	0·357

Table 2—continued

x/c	$\left(\frac{\partial^2 F}{\partial \eta^2}\right)_0$	$\left(\frac{\partial \Theta}{\partial \eta}\right)_0$	$^*\delta_1 Re_{m_x}^{\frac{1}{2}}/x$	$\delta_2 Re_{m_x}^{\frac{1}{2}}/x$	$C_{f_x} Re_{m_x}^{\frac{1}{2}}$	$Nu_x/Re_{m_x}^{\frac{1}{2}}$
			$T_w = 100, T_m = 0$			
0·0	2·060	1·535	0·827	0·437	0·440	1·040
0·2	1·925	1·504	0·865	0·452	0·409	1·012
0·4	1·774	1·468	0·909	0·469	0·374	0·981
0·6	1·602	1·424	0·959	0·488	0·336	0·946
0·8	1·404	1·370	1·020	0·509	0·292	0·903
1·0	1·171	1·299	1·096	0·532	0·242	0·850
1·2	0·883	1·202	1·194	0·559	0·181	0·781
1·4	0·489	1·039	1·342	0·589	0·099	0·669
1·5	0·160	0·848	1·479	0·606	0·033	0·544
1·520	0·000	0·673	1·550	0·610	0·000	0·432

Table 3. Circular cylinder, $u_m = u_0 \sin(x/c)$

x/c (*rad*)	$\left(\frac{\partial^2 F}{\partial \eta^2}\right)_0$	$\left(\frac{\partial \Theta}{\partial \eta}\right)_0$	$\delta_1 Re_{m_x}^{\frac{1}{2}}/x$	$\delta_2 Re_{m_x}^{\frac{1}{2}}/x$	$C_{f_x} Re_{m_x}^{\frac{1}{2}}$	$Nu_x/Re_{m_x}^{\frac{1}{2}}$
			$T_w = 0, T_m = 100$			
0·0	0·287	0·634	1·105	0·398	3·792	0·662
0·4	0·281	0·630	1·125	0·403	3·692	0·653
0·8	0·262	0·616	1·194	0·422	3·366	0·625
1·2	0·219	0·579	1·358	0·463	2·709	0·566
1·4	0·180	0·541	1·521	0·497	2·166	0·515
1·6	0·114	0·464	1·850	0·549	1·334	0·427
1·7	0·057	0·371	2·241	0·586	0·654	0·335
$1·742_5$	0·007	0·232	2·781	0·605	0·083	0·207
			$T_w = 100, T_m = 100$			
0·0	1·233	0·705	0·649	0·291	2·467	0·705
0·4	1·213	0·701	0·661	0·296	2·409	0·696
0·8	1·143	0·689	0·702	0·312	2·224	0·670
1·2	0·990	0·659	0·797	0·345	1·853	0·617
1·4	0·852	0·629	0·887	0·374	1·554	0·573
1·6	0·631	0·572	1·047	0·417	1·112	0·504
1·7	0·459	0·520	1·192	0·447	0·793	0·449
1·8	0·175	0·401	1·491	0·487	0·296	0·339
$1·820_5$	0·057	0·324	1·658	0·497	0·096	0·272

property Blasius velocity and thermal profiles at the leading edge are deformed by the adverse pressure gradient applied from the leading edge. However, in the case of the circular cylinder the variable fluid property profiles at the stagnation point are deformed first by the acceleration region $0 \leqslant x/c \leqslant \pi/2$ and then by the retarded region $x/c \geqslant \pi/2$, since $u_m = u_0 \sin(x/c)$.

5(a) *The flat plate*

Velocity and thermal profiles. Representative dimensionless velocity profiles for the extreme cases $(T_w, T_m) = (0, 100), (100, 100), (100, 0)$ and $(0, 0)$ are given graphically in Fig. 1 for various stations along the wall from the leading edge at $x = 0$ to the estimated position of separation $x = x_s$. The associated cooled wall thermal profiles are given in Fig. 2 and the heated wall

Table 4. Circular cylinder, $u_m = u_0 \sin(x/c)$

x/c (rad)	$\left(\frac{\partial^2 F}{\partial \eta^2}\right)_0$	$\left(\frac{\partial \Theta}{\partial \eta}\right)_0$	$\delta_1 Re_{m_x}^{\frac{1}{2}}/x$	$\delta_2 Re_{m_x}^{\frac{1}{2}}/x$	$C_{f_x} Re_{m_x}^{\frac{1}{2}}$	$Nu_x/Re_{m_x}^{\frac{1}{2}}$
			$T_w = 0, T_m = 0$			
0·0	1·233	1·488	0·649	0·291	2·467	1·488
0·4	1·213	1·480	0·661	0·296	2·409	1·470
0·8	1·143	1·448	0·702	0·312	1·224	1·409
1·2	0·990	1·373	0·797	0·345	1·853	1·286
1·4	0·852	1·298	0·887	0·374	1·554	1·183
1·6	0·631	1·159	1·047	0·417	1·112	1·021
1·7	0·459	1·029	1·192	0·447	0·713	0·889
1·8	0·175	0·736	1·491	0·487	0·296	0·622
$1·820_5$	0·057	0·540	1·658	0·496	0·096	0·454
			$T_w = 100, T_m = 0$			
0·0	4·060	1·804	0·300	0·157	1·227	1·728
0·4	4·008	1·797	0·305	0·160	1·203	1·710
0·8	3·831	1·774	0·324	0·170	1·126	1·653
1·2	3·443	1·718	0·365	0·190	0·975	1·541
1·4	3·100	1·663	0·402	0·208	0·854	1·453
1·6	2·562	1·569	0·461	0·235	0·683	1·325
1·8	1·614	1·367	0·575	0·277	0·412	1·107
1·9	0·723	1·104	0·697	0·308	0·180	0·872
1·935	0·063	0·762	0·801	0·321	$0·015_5$	0·596

thermal profiles in Fig. 3 both at the leading edge and point of separation; the constant fluid property thermal profiles for $(T_w, T_m) = (0, 0)$ and (100, 100) are also indicated. As the Görtler variables ξ and η are defined using the reference temperature T_m it is only permissible to compare profiles with the same small Reynolds number Re_{m_0}.

For the two sets of velocity profiles specified by $(T_w, T_m) = (0, 100)$ and (100,100) it is seen that the effect of cooling the wall moves the point of separation upstream, i.e. from $x_s/c = 0·959$ when $T_w = 100$ to $x_s/c = 0·677$ when $T_w = 0$. The reason for this is as follows. As the wall temperature decreases the shear stress across the boundary layer increases and this effect enhances the retardation effect of the main stream. Note that all of the cooled wall profiles have a point of inflexion. As already pointed out in [4] such profiles are probably unstable even at large Reynolds numbers. Quantitative information on these trends is available in Table 1. At any station, say $x/c = 0·4$, prior to separation, $(\partial^2 F/\partial \eta^2)_0$ decreases as T_w decreases from 100 to 0°C. There is, as expected, a corresponding increase in the skin friction coefficient C_{f_x}. An actual decrease in velocity will reduce the rate of heat transfer by convection hence giving the observed decrease in the thermal profiles for $(T_w, T_m) = (100, 100)$ (0, 100) as seen from Fig. 2. Note that the shape or exponential decay of the thermal profiles is controlled by the value of the main stream Prandtl number Pr_m (see [4]).

Consider the heated wall velocity profiles $(T_w, T_m) = (0, 0)$ and (100, 0) given in Fig. 1. Heating reduces the viscosity and hence the shear stress across the boundary-layer, leading to a local increase in velocity at any station. Thus the retardation effect of the main stream is opposed and the point of separation moves downstream of the constant fluid property location; with main stream temperature $T_m =$ 0°C x_s/c is located at 0·959 when $T_w = 0$°C, and

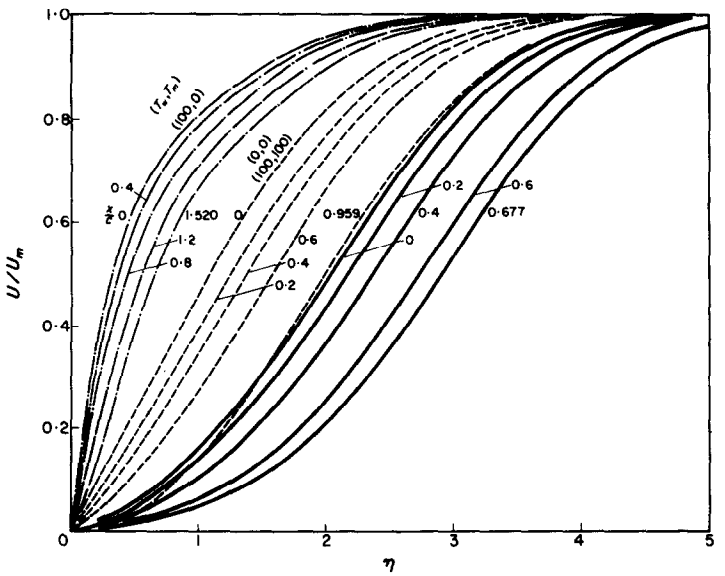

FIG. 1. Dimensionless velocity profiles for the flat plat with adverse pressure gradient $u_m = u_0\ (1 - x/8c)$. — · — $(T_w, T_m) = (100, 0)$; — — — (0, 0) or (100, 100); ——— (0, 100).

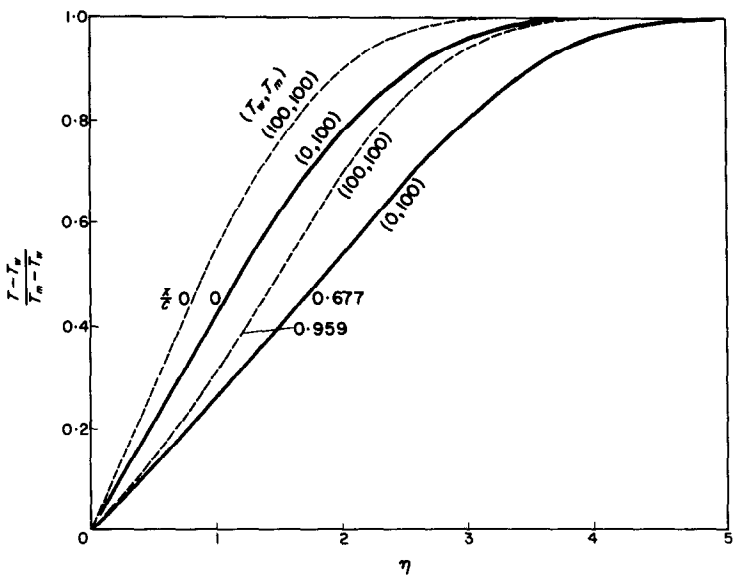

FIG. 2. Dimensionless cooled wall thermal profiles for $u_m = u_0\ (1 - x/8c)$. — — — $(T_w, T_m) = (100, 100)$; ——— (0, 100).

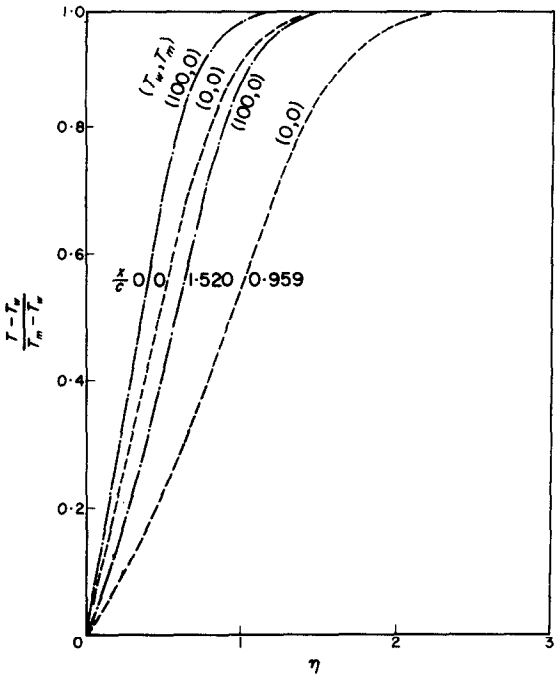

FIG. 3. Dimensionless heated wall thermal profiles for $u_m = u_0(1 - x/8c)$. — · — $(T_w, T_m) = (100, 0)$; ——— (0, 0).

at 1·520 when $T_w = 100°C$. Furthermore, the local increase in velocity leads to an increase in convective heat transfer giving the observed increase in the local temperature profiles as in Fig. 3 for $(T_w, T_m) = (100, 0)$ and (0, 0).

The above general trends on fluid velocity due to the effect of heating or cooling the wall are as expected, since the viscosity decreases with increasing temperature. It is interesting to note that the constant fluid property separation velocity profile at $x_s/c = 0{\cdot}959$ for $(T_w, T_m) = (100, 100)$ and the cooled wall Blasius profile at the leading edge ($x = 0$) for $(T_w, T_m) = (0, 100)$ overlap near the wall and are approximately equal at the outer edge of the fluid boundary layer. Finally the effect of heating or cooling the wall on the location of the separation point is adequately represented by the following correlation:

$$x_s/c = 0{\cdot}959 \left(\frac{Pr_m}{Pr_w}\right)^{\frac{1}{4}} \qquad (41)$$

This rather simple empirical result was obtained from the values of x_s/c given in Tables 1 and 2 by using the method of least squares.

Boundary-layer thicknesses. The dimensionless displacement and momentum thicknesses $\delta_{1_x} Re_{m_x}^{\frac{1}{2}}/x$ and $\delta_{2_x} Re_{m_x}^{\frac{1}{2}}/x$ as previously defined are given in Table 1 for a cooled wall and in Table 2 for a heated wall. Due to the adverse pressure gradient and resulting separation the boundary-layer thicknesses δ_{1_x} and δ_{2_x}, initially proportional to $\sqrt{x}$ at the leading edge, increase rapidly in the vicinity of the separation point. Heating the wall reduces the downstream growth of the boundary-layer thickness, whilst cooling the wall increases the rate of growth.

Skin friction and heat-transfer coefficients. The dimensionless group $C_{f_x} Re_{m_x}^{\frac{1}{2}}$ is tabulated for various combinations of the wall and main stream temperatures in Tables 1 and 2. For fixed main stream Reynolds number Re_{m_x} at any station prior to separation the skin friction coefficient increases with decreasing wall temperature. It is instructive to plot the scaled dimensionless quantity $C_{f_x} Re_{m_x}^{\frac{1}{2}}/C_{f_0} Re_{m_0}^{\frac{1}{2}}$ (i.e. the ratio of the local dimensionless group $C_{f_x} Re_{m_x}^{\frac{1}{2}}$ to its Blasius value at the leading edge) against x/x_s. For the limiting cases $(T_w, T_m) =$ (0, 100), (100, 100), (100, 0) and (0, 0), as given in Fig. 4, it is seen that the variable fluid property values for $C_{f_x} Re_{m_x}^{\frac{1}{2}}/C_{f_0} Re_{m_0}^{\frac{1}{2}}$ for all combinations of the wall and main stream temperatures are given accurately by the constant fluid property values. In the region $0 \leqslant x/x_s \leqslant 0{\cdot}95$ the error is at most 1 per cent and is probably greatest in the vicinity of the separation point. Thus the prediction of variable fluid property results for C_{f_x} from known constant fluid property results given in [6–8] is now possible, since the variable x/x_s, as a function of T_w and T_m, is known approximately from expression (41); values of $C_{f_0} Re_{m_0}^{\frac{1}{2}}$ and other flow and heat-transfer characteristics being available from [4].

In Fig. 5 the scaled dimensionless ratio $Nu_x Re_{m_x}^{-\frac{1}{2}}/Nu_0 Re_{m_0}^{-\frac{1}{2}}$ as a function of x/x_s is displayed for the cases $(T_w, T_m) = (0, 100)$, (100, 100), (100, 0) and (0, 0); note that the con-

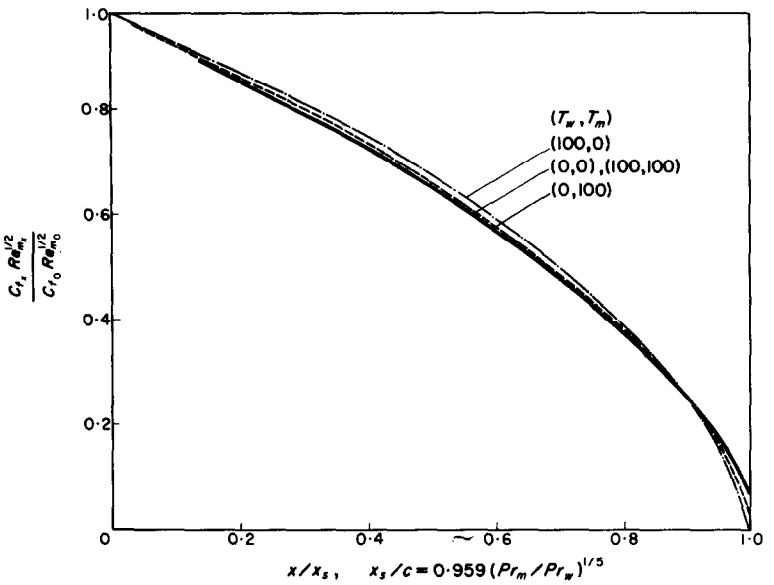

FIG. 4. Dimensionless skin friction coefficient $C_{f_x} Re_{m_x}^{\frac{1}{2}}/C_{f_0} Re_{m_0}^{\frac{1}{2}}$ for $u_m = u_0(1 - x/8c)$. — · — $(T_w, T_m) = (100, 0)$; — — — (0, 0) or (100, 100); ——— (0, 100).

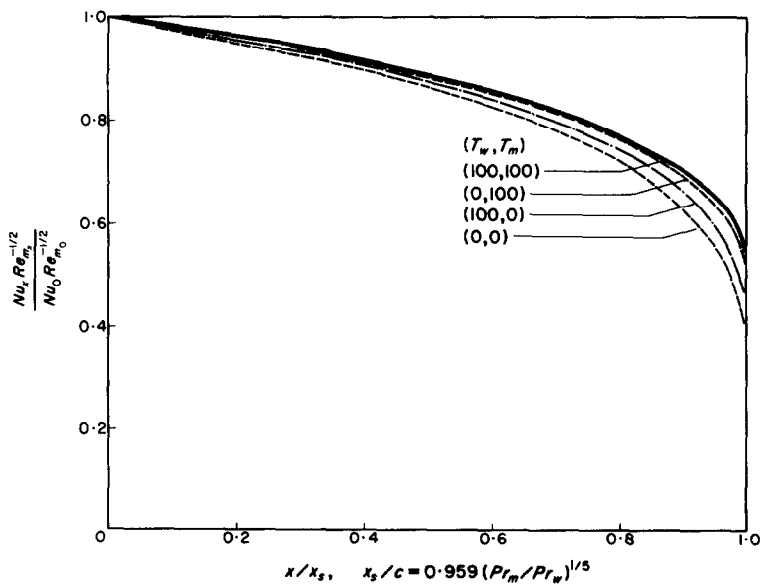

FIG. 5. Dimensionless Nusselt number $Nu_x Re_{m_x}^{-\frac{1}{2}}/Nu_0 Re_{m_0}^{-\frac{1}{2}}$ for $u_m = u_0(1 - x/8c)$. — · — $(T_w, T_m) = (100, 0)$; — — — (0, 0) or (0, 100); ——— (100, 100).

stant fluid property cases are limiting values as $T_w \to T_m$. For the cooled wall results with $T_m = 100°C$ and as T_w decreases from 100 to 0°C then $0{\cdot}56 \geqslant (Nu_s Re_{m_s}^{-\frac{1}{2}}/Nu_0 Re_{m_0}^{-\frac{1}{2}}) \geqslant 0{\cdot}48$; for the heated wall with $T_m = 0°C$ and as T_w increases from 0°C to 100°C then

$$0{\cdot}36 \leqslant (Nu_s Re_{m_s}^{-\frac{1}{2}}/Nu_0 Re_{m_0}^{-\frac{1}{2}}) \leqslant 0{\cdot}42.$$

Thus on using the variable x/x_s it is seen from Fig. 5 that variable fluid property cooled wall results are given accurately to within an error of 1 per cent in the interval $0 \leqslant x/c \leqslant 0{\cdot}95$ by the constant fluid property heat-transfer coefficients, but near separation the deviation is -14 per cent. In the case of the heated wall results this correlation, in view of the cooled wall results, is poor. Here the deviation at the separation point is $+16$ per cent and even at $x_s/c = 0{\cdot}8$ it is $+4$ per cent. Nevertheless the conclusion is that given the empirical result (41) it is possible to predict with accuracy either heated or cooled wall local skin friction and heat-transfer coefficients from known constant fluid property results; for the region $0 \leqslant x/x_s \leqslant 0{\cdot}8$ the deviation incurred would be at most 4 per cent.

5(b) *The circular cylinder*

Velocity and thermal profiles. The forward stagnation point, and the final separation point velocity profiles for the potential flow past a circular cylinder are displayed in Fig. 6 for wall and main stream conditions $(T_w, T_m) = (0, 100)$, (100, 100), (0, 0) and (100, 0). The associated cooled wall thermal profiles are given in Fig. 7 and the heated wall thermal profiles in Fig. 8.

Consider first the cooled wall results specified by $(T_w, T_m) = (0, 100)$ and (100, 100) with separation points located at $x_s/c = 1{\cdot}742$ and $1{\cdot}822$, respectively. In the region $0 \leqslant x \leqslant \pi/2$ the external flow is accelerated, and cooling the wall (and hence increasing the wall shear stress) has the effect of decreasing the acceleration in the boundary layer. After the pressure minimum at $x = \pi/2$ the external flow is retarded and cooling the wall enhances this effect. Thus the

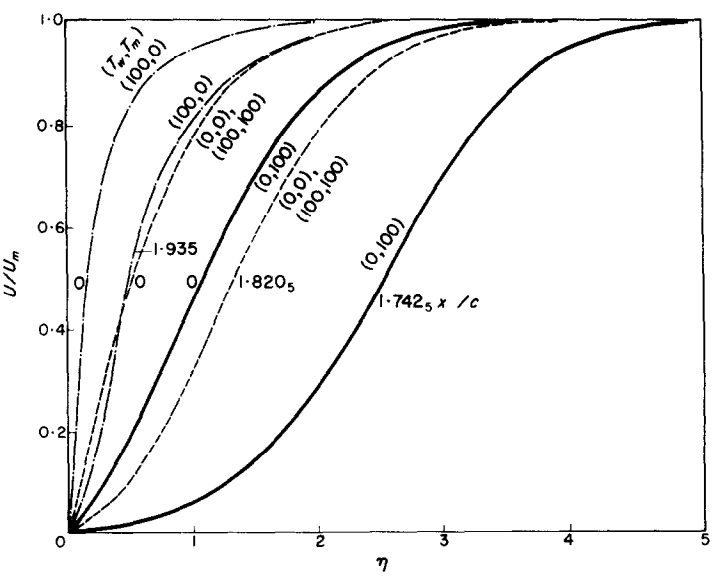

FIG. 6. Dimensionless velocity profiles for the cylinder with mainstream $u_m = u_0 \sin(x/c)$. — · — $(T_w, T_m) = (100, 0)$; — — — (0, 0) or (100, 100); ——— (0, 100).

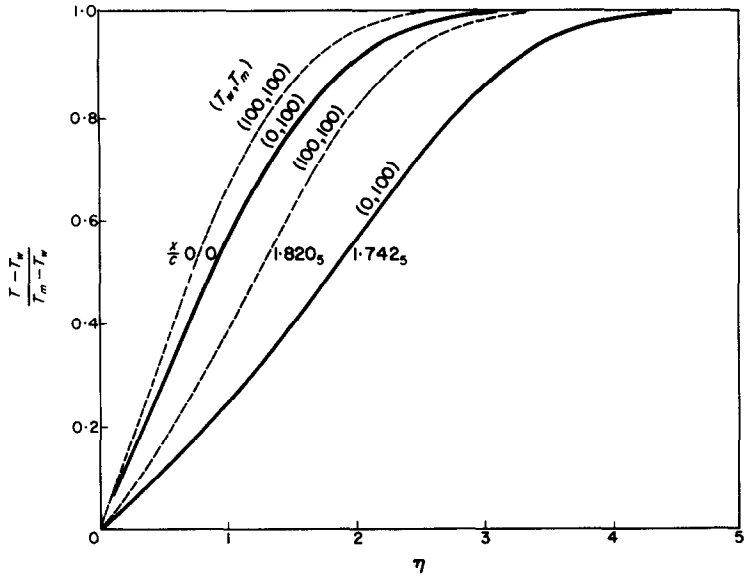

FIG. 7. Dimensionless cooled wall thermal profiles for $u_m = u_0 \sin(x/c)$. — — — $(T_w, T_m) = (100, 100)$; ——— (0, 100).

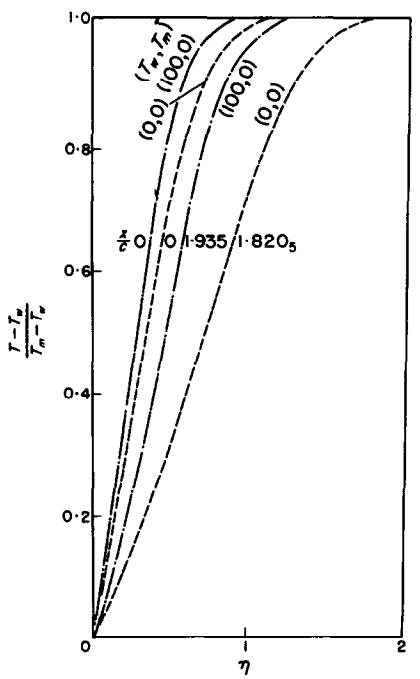

FIG. 8. Dimensionless heated wall thermal profiles for $u_m = u_0 \sin(x/c)$. — · — $(T_w, T_m) = (100, 0)$; — — — (0, 0).

effect of cooling the wall shifts the point of separation towards the forward stagnation point. In the case of the heated wall results specified by $(T_w, T_m) = (0, 0)$ and (100, 0) the separation points are $x_s/c = 1{\cdot}822$ and $1{\cdot}935$, respectively. Here heating the wall enhances the acceleration effect of the main stream in the region $0 \leqslant x/c \leqslant \pi/2$. Thus, there is a movement of the separation point away from the forward stagnation point.

It appears from these results that the effect of variable fluid properties on the location of the separation point is much less for the potential flow past a circular cylinder than in the case of the flat plate with main stream $u_m = u_0(1 - \frac{1}{8}x/c)$. However, the cylinder results can be compared, after the pressure minimum, with those of the flat plate. For, at $x/c = \pi/2$, the cylinder velocity profiles, if suitably scaled, are of the Blasius type. Clearly, for various wall and mainstream temperatures, the separation distance x_s for the flat plate must be related to the separation distance for the circular cylinder measured from $x/c = \pi/2$. This proves to be

true approximately since $(x_s/c - \pi/2)_{cyl}/(x_s/c)_{plate}$ takes the value 0·254, 0·260 and 0·240 for the wall and mainstream temperatures $(T_w, T_m) =$ (0, 100), (0, 0) or (100, 100) and (100, 0), respectively. Accepting the value 0·260 given by the constant fluid property model it follows, on using (41), that for the cylinder separation will occur when

$$\frac{x_s}{c} = \pi/2 + \frac{1}{4}\left(\frac{Pr_m}{Pr_w}\right)^{\frac{1}{3}} \tag{42}$$

Boundary-layer thicknesses. The dimensionless boundary-layer thicknesses $\delta_{1_x} Re_m^{\frac{1}{2}}/x$ and $\delta_{2_x} Re_{m_x}^{\frac{1}{2}}/x$ are given in Tables 3 and 4. At the stagnation point δ_1 and δ_2 are finite and increase slowly in the acceleration region. A small distance upstream of the pressure minimum the rate of growth increases rapidly up to the separation point. As in the flat plate solutions cooling the wall produces an increase in the rate of growth of the quantities; heating has the opposite effect.

Skin friction and heat-transfer coefficients. The dimensionless group $C_{f_x} Re_{m_x}^{\frac{1}{2}}$ is tabulated from the forward stagnation point to the separation point for various wall and main stream temperatures in Tables 3 and 4. Although $C_{f_x} Re_{m_x}^{\frac{1}{2}}$ decreases steadily from a finite value at the forward stagnation point to zero at the separation point, it must be remembered that the local shear stress τ_{w_x} is zero at $x = 0$, reaches a maximum at approximately $x_s/c = \pi/4$, and then decreases rapidly to zero at the separation point. In Fig. 9 the scaled dimensionless quantity $C_{f_x} Re_{m_x}^{\frac{1}{2}}$ is plotted against the variable x/x_s for the cases $(T_w, T_m) = (0, 100)$, (100, 100), (0, 0) and (100, 0). As in the flat plate solutions the variable fluid property results are closely approximated by the known constant fluid property values. Once the variable x/x_s is specified, using expression (42), variable fluid property results for $C_{f_x} Re_{m_x}^{\frac{1}{2}}/C_{f_0} Re_{m_0}^{\frac{1}{2}}$ can be deduced, except near to the separation point, from the constant fluid property model. For this reason the authors felt there was little justification in doing further calculations on the circular cylinder for other than the limiting wall and main stream temperatures listed.

The dimensionless heat-transfer characteristic $Nu_x Re_{m_x}^{-\frac{1}{2}}$ is tabulated in Tables 3 and 4 for $0 \leqslant x \leqslant x_s$ for various T_w and T_m. The dimensionless ratio $Nu_x Re_{m_x}^{-\frac{1}{2}}/Nu_0 Re_{m_0}^{-\frac{1}{2}}$ is displayed as a function of x/x_s in Fig. 10. Note that values of this ratio for wall and mainstream temperatures $(T_w, T_m) = (100, 0)$ and (0, 100) are coincident and are given graphically by a single curve. As in the skin friction coefficient the variable fluid property values are given, to within a few per cent by the constant fluid property model for the range $0 \leqslant x/x_s \leqslant 0{\cdot}9$.

ACKNOWLEDGEMENT

One of the authors (G.F.R.) is grateful to the Science Research Council for a maintenance grant.

REFERENCES

1. H. SCHUH, The solution of the laminar boundary-layer equation for the flat plate for velocity and temperature fields for variable physical properties and for the diffusion field at high concentration, NACA TM 1275 (1950).
2. R. A. SEBAN, The laminar boundary layer of a liquid with variable viscosity, in *Boelter Anniversary Volume, Heat Transfer, Thermodynamics and Education*, pp. 319–329. McGraw-Hill, New York (1964).
3. N. CURLE, *The Laminar Boundary Layer Equations*. Clarendon Press, Oxford (1962).
4. G. POOTS and G. F. RAGGETT, Theoretical results for variable property, laminar boundary layers in water, *Int. J. Heat Mass Transfer* **10**, 597–610 (1967).
5. K. STEWARTSON, *The Theory of Laminar Boundary Layers in Compressible Fluids*. Clarendon Press, Oxford (1964).
6. L. HOWARTH, On the solution of the laminar boundary-layer equations, *Proc. R. Soc.* **A164**, 547–579 (1933).
7. D. R. HARTREE, A solution of the laminar boundary-layer equation for retarded flow, *Rep. Memo. Aeronaut. Res. Comm. (Coun.)* **2426** (Spec. Vol. II) (1939).
8. D. C. LEIGH, The laminar boundary-layer equation: a method of solution by means of automatic computer, *Proc. Camb. Phil. Soc.* **51**, 320–332 (1955).
9. S. GOLDSTEIN, On laminar boundary layer flow near a position of separation, *Q. Jl Mech. Appl. Math.* **1**, 43–69 (1948).
10. C. W. JONES, On a solution of the laminar boundary-layer equation near a position of separation, *Q. Jl Mech. Appl. Math.* **1**, 385–407 (1948).
11. R. M. TERRILL, Laminar boundary-layer flow near separation with and without suction, *Phil. Trans. R. Soc.* **A253**, 55–100 (1960).

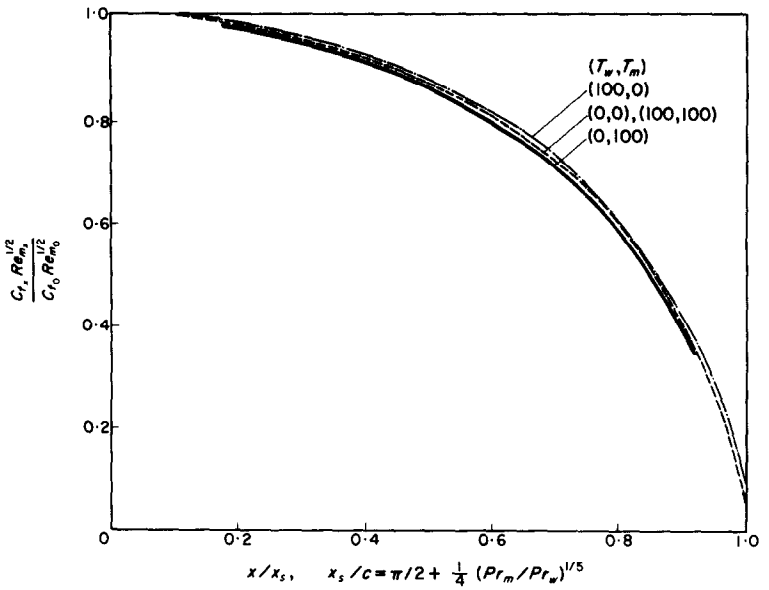

FIG. 9. Dimensionless skin friction coefficient for $u_m = u_0 \sin(x/c)$. — · — $(T_w, T_m) = (100, 0)$; — — — (0, 0) or (100, 100); ——— (0, 100).

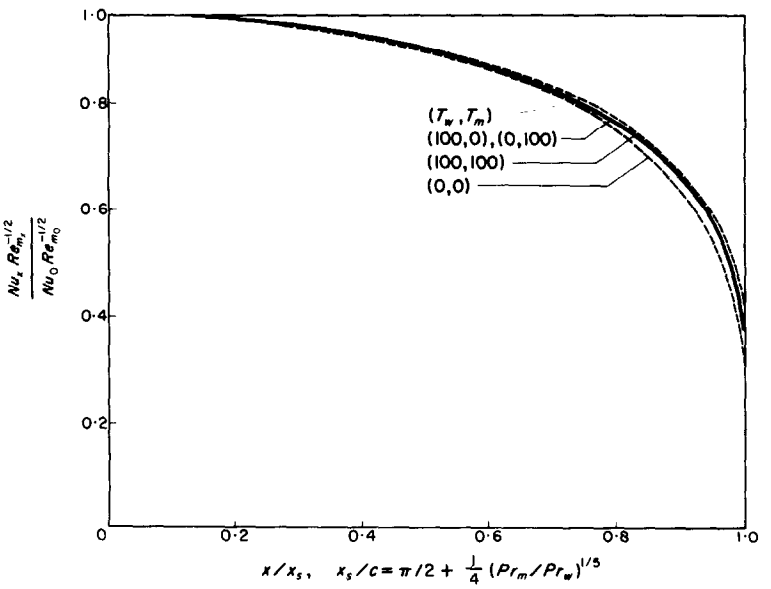

FIG. 10. Dimensionless Nusselt number $Nu_x Re_x^{-\frac{1}{2}}/Nu_0 Re_0^{-\frac{1}{2}}$ for $u_m = u_0 \sin(x/c)$. — — — $(T_w, T_m) = (100, 100)$ or (0, 0); ——— (100, 0) or (0, 100).

12. K. STEWARTSON, On Goldstein's theory of laminar separation, *Q. Jl Mech. Appl. Math.* **11**, 399–410 (1958).
13. N. B. CURLE, The steady compressible laminar boundary layer, with arbitrary pressure gradient and uniform wall temperature. *Proc. R. Soc.* **A249**, 206–224 (1959).
14. G. POOTS, A solution of the compressible laminar boundary-layer equations with heat transfer and adverse pressure gradient, *Q. Jl Mech. Appl. Math.* **13**, 57–84 (1960).
15. K. STEWARTSON, The behaviour of the laminar compressible boundary layer near a point of zero skin friction, *J. Fluid. Mech.* **12**, 117–128 (1962).
16. Y. R. MAYHEW and G. F. C. ROGERS, *Thermodynamic and Transport Properties of Fluids* (MKS Units). Blackwell, Oxford (1964).
17. G. POOTS and M. H. ROGERS, Laminar flow between parallel flat plates, with heat transfer, of water with variable physical properties, *Int. J. Heat Mass Transfer* **8**, 1515–1535 (1965).
18. J. CRANK and P. NICOLSON, A practical method for numerical evaluation of solutions of partial differential equations of the heat conduction type, *Proc. Camb. Phil. Soc.* **43**, 50–67 (1947).

APPENDIX

Numerical Solution of the Boundary-Layer Equations

The numerical procedure for the solution of the basic equations was programmed in Algol and computations completed on the Atlas Computer at Harwell.

The procedure for solving the transformed equations (10) and (11) with the relevant boundary conditions was developed by Hartree and Womersley (see Hartree [7]). This implicit method is basically that proposed by Crank and Nicolson [18] for the integration of the linear transient heat conduction equation; the latter being a convergent and stable process for all finite values of the relevant mesh lengths.

The Hartree–Womersley method has been applied to various boundary-layer investigations (see for example [7, 8, 11]). Derivatives in the ξ-direction are replaced by backward difference formulae (without truncation error) and all other quantities by averages. The partial differential equations are reduced to the solution, at any station ξ_{i+1} along the wall, of a pair of non-linear coupled ordinary differential equations whose coefficients are dependent on the known solution at the previous station ξ_i. Central difference relations are used to approximate derivatives in the η-direction. An iterative matrix scheme, to be described, is employed to solve these equations.

Suppose that the velocity and thermal field functions F and Θ are available at the station ξ_i. It is required to evaluate these functions at the next downstream station ξ_{i+1}. Working in terms of the new velocity field function

$$q = \partial F/\partial\eta, \tag{43}$$

equations (10) and (11) are approximated by

$$\left\{\frac{(\rho\mu)^{(M)}_{i+1,j}}{(\rho\mu)_m}\,q^{(M+1)\prime}_{i+1,j}\right\}' - q^{(M+1)}_{i+1,j}(\lambda+\beta_{i+1})\,q^{(M)}_{i+1,j} + (\tfrac{1}{2}-\lambda)\,q^{(M+1)}_{i+1,j}\int_0^{\eta_j} q_i\,\mathrm{d}\eta + (\tfrac{1}{2}+\lambda)\,q^{(M+1)\prime}_{i+1,j}\int_0^{\eta_j} q^{(M)}_{i+1}\,\mathrm{d}\eta$$

$$+\frac{h}{2}(\tfrac{1}{2}+\lambda)\,(q^{(M+1)}_{i+1,j}+q^{(M+1)}_{i+1,j-1})\,q'_{i,j} = -\left[(\tfrac{1}{2}+\lambda)\,q'_{i,j}\int_0^{\eta_{j-1}} q^{(M)}_{i+1}\,\mathrm{d}\eta + \left\{\frac{(\rho\mu)_{i,j}}{(\rho\mu)_m}\,q'_{i,j}\right\}'\right.$$

$$\left.+(\tfrac{1}{2}-\lambda)\,q'_{i,j}\int_0^{\eta_j} q_i\,\mathrm{d}\eta + (\lambda-\beta_i)\,q^2_{i,j} + \beta_i\frac{\rho_m}{\rho_{i,j}} + \beta_{i+1}\frac{\rho_m}{\rho_{i+1,j}}\right], \tag{44}$$

and

$$\left\{\frac{(\rho k)_{i+1,j}^{(M)}}{(\rho k)_m}\Theta_{i+1,j}^{(M+1)\prime}\right\}' + \frac{1}{2}\frac{Pr_m}{c_{p_m}}(c_{p_{i,j}} + c_{p_{i+1,j}}^{(M)})\left[(\tfrac{1}{2}-\lambda)\Theta_{i+1,j}^{(M+1)\prime}\int_0^{\eta_j} q_i\,d\eta + (\tfrac{1}{2}+\lambda)\Theta_{i+1,j}^{(M+1)\prime}\int_0^{\eta_j} q_{i+1}\,d\eta\right.$$
$$\left. - \lambda(q_{i,j} + q_{i+1,j})\Theta_{i+1,j}^{(M+1)}\right]$$
$$= -\left[\left(\frac{(\rho k)_{i,j}}{(\rho k)_m}\Theta_{i,j}'\right)' + \frac{1}{2}\frac{Pr_m}{c_{p_m}}(c_{p_{i,j}} + c_{p_{i+1,j}}^{(M)})\left\{(\tfrac{1}{2}-\lambda)\Theta_{i,j}'\int_0^{\eta_j} q_i\,d\eta\right.\right.$$
$$\left.\left. + (\tfrac{1}{2}+\lambda)\Theta_{i,j}'\int_0^{\eta_j} q_{i+1}\,d\eta + \lambda(q_{i,j}+q_{i+1,j})\Theta_{i,j}\right\}\right] \tag{45}$$

respectively, at the $(i+1,j)$th mesh point. Here $h = \eta_{j+1} - \eta_j$ is the mesh length in the η-direction,

$$\lambda = \frac{\xi_{i+1} + \xi_i}{\xi_{i+1} - \xi_i},$$

and the prime denotes differentiation with respect to η. The superscript M is used to denote the Mth iterate. Derivatives in the η-direction are now replaced by truncated central differences formula, as in the following

$$\left(\frac{\rho\mu}{(\rho\mu)_m}q_{i,j}'\right)' = \frac{1}{h^2}\left\{\frac{(\rho\mu)_{i,j+\frac{1}{2}}}{(\rho\mu)_m}q_{i,j+1} - \frac{(\rho\mu)_{i,j+\frac{1}{2}} + (\rho\mu)_{i,j-\frac{1}{2}}}{(\rho\mu)_m}q_{i,j} + \frac{(\rho\mu)_{i,j-\frac{1}{2}}}{(\rho\mu)_m}q_{i,j-1}\right\}, \tag{46}$$

and the integrals are evaluated by quadrature using the trapezoidal rule as in

$$\int_0^{\eta_j} q_i\,d\eta = h(q_{i,1} + q_{i,2} + \ldots + q_{i,j-1} + \tfrac{1}{2}q_{i,j}). \tag{47}$$

On using relations of the type (46) and (47) the left-hand side of (44) contains, in general, three unknown and the right-hand side three known pivotal values of q; similarly for equation (45). Let N be the number of mesh points in the η-direction. It is required to solve the coupled non-linear pair of N simultaneous equations in $q_{i+1,j}$ and $\Theta_{i+1,j}$ for $j = 1, 2, \ldots N$ in terms of the N known pivotal values of $q_{i,j}$ and $\Theta_{i,j}$.

Both the velocity and thermal equations (44) and (45) can now be expressed in terms of the following band matrix scheme. The first equation ($j = 1$) is

$$-L_1^{(M)}X_{i+1,1}^{(M+1)} + L_2^{(M)}X_{i+1,2}^{(M+1)} = P_1^{(M)}, \tag{48}$$

and for $j = 2, 3, \ldots N$,

$$L_{j-1}^{(M)}\ X_{i+1,j-1}^{(M+1)} - L_j^{(M)}X_{i+1,j}^{(M+1)} + L_{j+1}^{(M)}X_{i+1,j+1}^{(M+1)} = -P_j^{(M)}. \tag{49}$$

For the velocity field:

$$X_{i+1,j} = q_{i+1,j}, X_{i+1,0} = 0, X_{i+1,N+1} = 1, \tag{50}$$

and the vectors L and P are defined by:

$$L_{j-1} = \frac{(\rho\mu)_{i+1,j}^{-\frac{1}{2}}}{(\rho\mu)_m} - \tfrac{1}{2}h^2(\tfrac{1}{2} - \lambda)\,\alpha_{i,j} + \tfrac{1}{4}h^2(\tfrac{1}{2} + \lambda)(q_{i,j+1} - q_{i,j-1}) - \tfrac{1}{2}h^2(\lambda + \tfrac{1}{2})\,\alpha_{i+1,j}, \tag{51}$$

$$L_j = \frac{(\rho\mu)_{i+1,j+\frac{1}{2}} + (\rho\mu)_{i+1,j-\frac{1}{2}}}{(\rho\mu)_m} - \tfrac{1}{4}h^2(\tfrac{1}{2} + \lambda)(q_{i,j+1} - q_{i,j-1}) + h^2(\lambda + \beta_{i+1})\,q_{i+1,j}, \tag{52}$$

$$L_{j+1} = \frac{(\rho\mu)_{i+1,j+\frac{1}{2}}}{(\rho\mu)_m} + \tfrac{1}{2}h^2(\tfrac{1}{2} - \lambda)\,\alpha_{i,j} + \tfrac{1}{2}h^2(\tfrac{1}{2} + \lambda)\,\alpha_{i+1,j}, \tag{53}$$

$$P_j = \frac{(\rho\mu)_{i,j+\frac{1}{2}}}{(\rho\mu)_m} q_{i,j+1} - \frac{(\rho\mu)_{i,j+\frac{1}{2}} + (\rho\mu)_{i,j-\frac{1}{2}}}{(\rho\mu)_m} q_{i,j} + \frac{(\rho\mu)_{i,j-\frac{1}{2}}}{(\rho\mu)_m} q_{i,j-1} + \tfrac{1}{2}h^2(\tfrac{1}{2} - \lambda)(q_{i,j+1} - q_{i,j-1})\,\alpha_{i,j}$$
$$+ \tfrac{1}{2}h^2(\tfrac{1}{2} + \lambda)(q_{i,j+1} - q_{i,j-1})\,\alpha_{i+1,j-1} + \tfrac{1}{2}h^2(\tfrac{1}{2} + \lambda)(q_{i,j+1} - q_{i,j-1})\,\alpha_{i+1,j-1} + h^2(\lambda - \beta_i)\,q_{i,j}^2$$
$$+ h^2(\beta_i s_{i,j} + \beta_{i+1} s_{i+1,j}), \tag{54}$$

where

$$\alpha_{N,j} = q_{N,1} + q_{N,2} + \ldots + q_{N,j-1} + \tfrac{1}{2}q_{N,j}, \tag{55}$$

and

$$s_{i,j} = \rho_m/\rho_{i,j}. \tag{56}$$

Similarly for the temperature field:

$$X_{i+1,j} = \Theta_{i+1,j}, X_{i+1,0} = 0, X_{i+1,N+1} = 1, \tag{57}$$

$$L_{j-1} = \frac{(\rho k)_{i+1,j-\frac{1}{2}}}{(\rho k)_m} - \frac{h^2}{4}\frac{Pr_m}{c_{p_m}}(c_{p_{i,j}} + c_{p_{i+1,j}})\left[(\tfrac{1}{2} - \lambda)\,\alpha_{i,j} + (\tfrac{1}{2} + \lambda)\,\alpha_{i+1,j}\right], \tag{58}$$

$$L_j = \frac{(\rho k)_{i+1,j+\frac{1}{2}} + (\rho k)_{i+1,j-\frac{1}{2}}}{(\rho k)_m} + \tfrac{1}{2}\lambda h^2\frac{Pr_m}{c_{p_m}}(c_{p_{i,j}} + c_{p_{i+1,j}})(q_{i+1,j} + q_{i+1,j}), \tag{59}$$

$$L_{j+1} = \frac{(\rho k)_{i+1,j+\frac{1}{2}}}{(\rho k)_m} + \frac{h^2}{4}\frac{Pr_m}{c_{p_m}}(c_{p_{i,j}} + c_{p_{i+1,j}})\left[(\tfrac{1}{2} - \lambda)\,\alpha_{i,j} + (\tfrac{1}{2} + \lambda)\,\alpha_{i+1,j}\right], \tag{60}$$

and finally

$$P_j = \frac{(\rho k)_{i,j+\frac{1}{2}}}{(\rho k)_m}\Theta_{i,j+1} - \frac{(\rho k)_{i,j+\frac{1}{2}} + (\rho k)_{i,j-\frac{1}{2}}}{(\rho k)_m}\Theta_{i,j} + \frac{(\rho k)_{i,j-\frac{1}{2}}}{(\rho k)_m}\Theta_{i,j-1} + \tfrac{1}{2}h^2\frac{Pr_m}{c_{p_m}}(c_{p_{i,j}} + c_{p_{i+1,j}})$$
$$\times \left[\tfrac{1}{2}(\tfrac{1}{2} - \lambda)\,\Theta_{i,j+1} - \Theta_{i+1,j})\,\alpha_{i,j} + \tfrac{1}{2}(\tfrac{1}{2} + \lambda)(\Theta_{i,j+1} - \Theta_{i,j-1})\,\alpha_{i+1,j} + \lambda(q_{i,j} + q_{i+1,j})\,\Theta_{i,j}\right]. \tag{61}$$

The iterative scheme used to solve the nonlinear simultaneous equations (48) and (49) for the velocity and thermal field functions is now described. $q_{i,j}$ and $\Theta_{i,j}$ for $j = 1, 2, \ldots, N$ are known and as a first approximation for the velocity field the elements $L^{(0)}_{j-1}$, $L^{(0)}_{j}$, $L^{(0)}_{j+1}$ of the band matrix and the right-hand side elements $P^{(0)}_{j}$ [as given by expressions (52–54)] are computed assuming that $q^{(0)}_{i+1,j} = q_{i,j}$ and $\Theta_{i+1,j} = \Theta^{(0)}_{i,j} =$.* The X-vector is computed from the band matrix (48) and (49) using the Choleski method. Thus a new estimate $q^{(1)}_{i+1,j}$ is known. With the same $\Theta^{(0)}_{i,j}$ the process is repeated for the calculation of $q^{(M)}_{i+1,j}$ with $M = 2$, 3, 4 and etc. until there is no further change in current values. For this estimate of $q_{i+1,j}$ the iterative procedure is now applied to the thermal field equations [as defined by (57–61)] giving, for the current values of $q_{i+1,j}$, a new estimate of $\Theta_{i+1,j}$. This iterative subroutine, for the calculation of $q_{i+1,j}$ and $\Theta_{i+1,j}$ is again repeated until some overall test on accuracy is automatically satisfied.

The integration is started at $\xi = 0$. For the flat plate with $u_m = u_0(1 - x/8c)$, $q_0(\eta) = f'(\eta)$ and $\Theta_0(\eta) = \theta(\eta)$, the variable fluid property Blasius functions are already available from [1]. The programme involving the above iterative matrix schemes was tested on the known velocity field solutions for $(T_w, T_m) = (0, 0)$ and $(100, 100)$; at the same time the thermal fields for $Pr_m =$ 13·621 and 1·737 were obtained. For these, as already discussed, the numerical process breaks down near $x = x_s$ due to the algebraic singularity at this point. Indeed, as the velocity field is not analytic at x_s finite differences will no longer be meaningful. Moreover, the actual assumptions of boundary-layer theory are no longer valid in the upstream neighbourhood of x_s, since $(\partial u/\partial y)_w$ is small. Variable fluid property calculations were then attempted and as in the constant fluid property case the numerical process failed to converge at some critical distance x_s, when $(\partial u/\partial y)_w$ was small. It has not, however, been established analytically that this behaviour is due to an algebraic singularity at x_s and this question remains unanswered at present. Due to the labour and more important still the expense involved in obtaining the numerical results when the wall shear stress is small, the programme was terminated when x_s was known to three significant figures. For example in the worst case for the flat plate with $T_w = 0$ and $T_m = 100°C$ to approach the quoted value of $x_s/c = 0{\cdot}677$ a mesh length in the ξ-direction of 0·001 is required from 0·665 onwards; at $x_s/c = 0{\cdot}677$ the value of $(\partial^2 F/\partial\eta^2)_0$ had then decreased to only 7 per cent of its value at the leading edge. Furthermore, the actual Atlas computing time for $N = 60$, $h = 0{\cdot}1$, per step in the ξ-direction, was usually at most a minute.

In the solutions for the potential flow past a circular cylinder with $u_m = u_0 \sin(x/c)$ the initial functions $q_0 = f'(\eta)$ and $\Theta_0 = \theta(\eta)$ relating to the variable fluid property two-dimensional stagnation point, defined by equations (23, 24, 19), were required. These were computed using the basic iterative scheme already incorporated in the programme written for the Hartree–Womersley procedure. The integrations from $x = 0$ to x_s for $(T_w, T_m) = (0, 0)$ or $(100, 100)$ were found to be in excellent agreement with those of Terrill [11]. Due to the acceleration region from $x/c = 0$ to $\pi/2$ the number of steps taken in the ξ-direction for the variable fluid property solutions was of the order of fifty.

* In general, information is known at stations upstream of ξ_{i+1} and a better estimate is

$$q_{i+1,j} = q_{i,j} + \frac{\xi_{i+1} - \xi_i}{\xi_i - \xi_{i-1}}(q_{i,j} - q_{i-1,j}),$$

together with a similar expression for $\Theta_{i+1,j}$.

Résumé—On présente des solutions numériques des équations de la couche limite laminaire bidemensionelle pour des écoulements d'eau avec transport de chaleur et gradient de pression contraire. Les valeurs expérimentales (dans la gamme 0 à 100°C) de la viscosité, de la conductivité, de la chaleur spécifique et de la masse volumique sont utilisées. En introduisant les transformations de Howarth–Dorodnitsyn et de Görtler, les équations de la couche limite sont mises sous une forme convenable pour l'analyse

numérique. La paire d'équations aux dérivées partielles couplées qui en résulte sont résolues, en employant la méthode implicite de Hartree et Womersley, d'abord pour l'écoulement le long d'une plaque plane avec une vitesse de l'écoulement principal $u_m = u_0\ (1 - x/8c)$ et ensuite pour l'écoulement potentiel le long d'un cylindre circulaire avec une vitesse de l'écoulement principal $u_m = u_0 \sin (x/c)$. Les caractéristiques de la couche limite telles que les épaisseurs de déplacement et de quantité de mouvement, les coefficients de frottement pariétal et de transport de chaleur sont évalués jusqu'au point de décollement. L'effet de la variation des propriétés du fluide consiste en un déplacement de la position du décollement vers l'amont ou vers l'aval de l'endroit connu correspondant à l'écoulement incompressible isotherme selon que la paroi est refroidie ou réchauffée. Par exemple, avec une vitesse de l'écoulement principal de la forme $u_m = u_0\ (1 - x/8c)$, les résultats numériques montrent que le décollement se produit vraisemblablement pour approximativement $x_s/c = 0{,}959\ (Pr_m/Pr_w)^{\frac{1}{4}}$. Dans le cas où $u_m = u_0 \sin (x/c)$, l'endroit approximatif est donné par $x_s/c = \pi/2 + 0{,}25\ (Pr_m/Pr_w)^{\frac{1}{4}}$. Ici Pr_w et Pr_m sont, respectivement, les nombres de Prandtl à la paroi et dans l'écoulement principal.

Zusammenfassung—Numerische Lösungen von zweidimensionalen laminaren Grenzschichtgleichungen für Strömungen mit Wärmeübergang und gegenläufigen Druckgradienten werden für Wasser angegeben. Versuchswerte (im Bereich 0–100°C) für Zähigkeit, Wärmeleitfähigkeit, spezifische Wärme und Dichte werden verwendet. Durch Einführung der Howarth–Dorodnitsyn und Görtler Transformation werden die Grenzschichtgleichungen in eine für die numerische Bearbeitung passende Form gebracht. Das sich ergebende Paar von gekoppelten partiellen Differential-gleichungen wird gelöst mit Hilfe der impliziten Methode von Hartree und Womersley; 1. für die Strömung entlang einer ebenen Platte mit einer Strömungsgeschwindigkeit $u_m = u_0\ (1 - x/8c)$ und 2. für die Potentialströmung entlang eines Kreiszylinders mit der Hauptstromgeschwindigkeit $u_m = u_0 \sin (x/c)$.

Grenzschicht-Charakteristika wie Verdrängungs- und Impulsdicke, Wandreibung und Wärmeübergangskoeffizient werden bis zum Ablösepunkt und Wärmeübergangskoeffizient werden bis zum Ablösepunkt bestimmt. Der Einfluss veränderlicher Stoffwerte besteht darin, den Ort der Ablösung stromauf- oder stromabwärts vom bekannten Ort für inkompressible isotherme Strömung zu verlagern, jenachdem, ob die Wand gekühlt oder beheizt ist. Für die Hauptstromgeschwindigkeit $u_m = u_0\ (1 - x/8c)$ beispielsweise ergibt sich in der numerischen Auswertung die Ablösung etwa an der Stelle $x_s/c = 0{,}959\ (Pr_m/Pr_w)^{\frac{1}{4}}$ Hier bedeuten $Pr_w - Pr_m$ die Wand-und die Hauptstrom-Prandtlzahlen.

Аннотация—Для воды приводятся численные решения двухмерных уравнений ламинарного пограничного слоя течений при наличии теплообмена и отрицательного градиента давления. Используются экспериментальные значения (от 0 до 100°C) вязкости, теплопроводности, удельной теплоты и плотности. Введение преобразований Ховарта–Дородницына и Гёртлера приводит уравнения пограничного слоя к виду, удобному для вычислений. С помощью неявного метода Хартри и Уомерсли решается результирующая пара взаимосвязанных дифференциальных уравнений в цастных производных, вопервых, для плоской пластины в потоке при скорости основного потока $u_m = u_0(1 - x/8c)$ и, вовторых, для круглого цилиндра в безвихревом потоке при скорости основного потока $u_m = u_0 \cdot \sin (x/c)$. Характеристики пограничного слоя такие как: толщина вытеснения, толщина потери импульса, коэффициенты поверхностного трения и теплообмена определяются до точек отрыва. Влияние переменных свойств жидкости заключается в перемещении положения точки отрыва вверх иливниз по течению по сравнению с изветсным положением этой точки в случае несжимаемого изотермического потока в зависимости от того нагревается стенка или охлаждается. Например, при скорости основного потока $u_m = u_0(1 - x/8c)$ полученные численные результаты показывают, что отрыв происходит приблизительно при $x_s/c = 0{,}959(pr_m/pr_w)^{\frac{1}{4}}$. Для случая $u_m = u_0 \cdot \sin (x/c)$ приближенное расположение зоны отрыва определяется $x_s/c = \pi/2 + 0{,}25 \times (pr_m/pr_w)^{\frac{1}{4}}$. Здесь pr_w и pr_m — числа Прандтля для стенки и основного потока, соответсвенно.